Int. J. Electrochem. Sci., 16 **(2021)** Article Number: 211060, doi: 10.20964/2021.10.51

International Journal of
ELECTROCHEMICAL
SCIENCE
www.electrochemsci.org

Corrosion and Interfacial Behavior of FeSi Alloy in Organic Electrolyte Solutions

Huaiyu Zhong[1], *Qingdong Zhong*[1,3,*], *Jian Yang*[1], *Xiaofen Wang*[1], *Yan Shi*[1], *Shengwen Zhong*[2,*], *Xiaojin Li*[4]

[1] State Key Laboratory of Advanced Special Steel, School of Materials Science and Engineering, Shanghai University, Shanghai, 200444, People's Republic of China;
[2] Faculty of Materials Metallurgy and Chemistry, Jiangxi University of Science and Technology, Ganzhou, Jiangxi, 341000, People's Republic of China;
[3] Panzhihua University, Panzhihua, Sichuan, 617000, People's Republic of China;
[4] Zhuhai Guangrui New Material Co., Ltd. Zhuhai, Guangdong, 519000, People's Republic of China.
[*]E-mail: qdzhong@shu.edu.cn, zqd9391a@126.com

Received: 2 July 2021 / *Accepted:* 12 August 2021 / *Published:* 10 September 2021

The corrosion and interfacial behavior of FeSi alloy in organic electrolyte was investigated using gravimetric and electrochemical methods. The results indicated that the corrosion rate at 10 days reduced approximately 44.71% on the first day. Electrochemical and gravimetric data were consistent, indicating a decreasing corrosion rate with increasing immersion time. The main corrosion behavior of FeSi alloy was the dissolution of Fe. The results showed that PF_6^- corroded Fe to Fe (II) that further evolved into Fe (III), forming fluoride films (FeF_3) on the alloy surface, which would reduce the contact area between the material and electrolyte, and preventing the corrosive electrolyte from further corroding the FeSi alloy substrate. Hence, the occurrence of corrosion was slowed down or inhibited, and the electrochemical performance of FeSi alloy was more stable in $LiPF_6$ solution. The formation of iron (III) fluoride was also confirmed via X-ray photoelectron spectroscopy analysis.

Keywords: Corrosion behavior, FeSi alloy, $LiPF_6$, lithium-ion battery

1. INTRODUCTION

Lithium ion batteries (LIBS) have been widely studied and used in the field of consumer electronics in recent years, owning to their high energy and power density, long cycle life and environmental friendliness[1, 2]. Silicon (Si) has attracted wide attention because of its high theoretical specific capacity and is considered one of the most promising anode materials for lithium-ion batteries[3-8]. However, Si undergoes a substantial volume change during lithium insertion and delithiation

reactions, resulting in mechanical failure of the active material; and a reduction in charge and discharge efficiency as well as a rapid reduction in cycle performance[9-11].

FeSi alloy is a promising anode material for lithium-ion batteries because Fe has excellent ductility and electrical conductivity, and the lithium-embedded inert alloy phase can be obtained as a buffer matrix to buffer the volume change of Si. Using the characteristics of metals to mitigate the volume change is an effective method. The addition of Fe can reduce the resistivity and volume expansion of silicon. With an increase in Fe content, the volume expansion rate of Si gradually decreases[12, 13]. In addition, $FeSi_x$ alloy phase will be formed after alloying, which acts as an inert phase embedded with lithium to buffer the volume change of silicon. Meanwhile, the relatively strong conductivity of the FeSi2 phase can also improve the electrochemical properties of the material [14, 15]. However, although Fe is inactive in the lithium insertion/delithiation process, it may be electrochemically active in the presence of water and solvent, making it susceptible to corrosion.

As a water-sensitive compound, lithium hexafluorophosphate ($LiPF_6$) is commonly used as a lithium salt in lithium-ion electrolytes[16]. Ethylene carbonate (EC) or diethyl carbonate (DEC) is typically used as a solvent[17, 18]. Previous studies on electrolyte corrosion mainly focused on the container and current collectors. Guitian et al.[19] found that the corrosion product layer of iron in an electrolyte was porous. Li et al.[20] studied the mechanisms of Al corrosion in LiFSI-based electrolytes at 45 °C. The irregular, loose, and unprotected AlF_3 materials due to the dissolution of co-generated Al $(FSI)_3$ can exacerbate Al corrosion with an increase in temperature. Chen et al.[21] reported that asymmetrical rolling and surface morphology modification of copper foils can effectively improve corrosion performance. However, electrochemical reaction between the active material and electrolyte is usually neglected and seldom studied. The side reaction between the active material and electrolyte is also an essential factor causing electrode failure. The phenomena degrade the performance of lithium-ion batteries because of the degradation of the electrolyte and active materials.

In this work, the corrosion mechanism and interfacial behavior of FeSi alloy were investigated in organic electrolyte solution. The corrosion process of FeSi alloy in organic electrolyte solutions was investigated using gravimetric analysis, electrochemical performance, and surface morphology. The effects of anionic substances on the electrochemical performance of FeSi alloys were discussed in detail via X-ray photoelectron spectroscopy (XPS) analysis.

2. EXPERIMENTAL

2.1 Materials and methods

FeSi alloy was produced at Hunan Shanglin New Material Technology Co., Ltd. The chemical composition of the FeSi alloy is shown in Table 1. First, the FeSi alloy *(*10 mm × 10 mm × 2 mm*)* was sealed with epoxy resin. Then, the testing surface was mechanically grinded with 400 – 2000 grain size *SiC* paper and polished with 1 to 9 μm size diamond suspension, followed by ultrasonic cleaning using ethanol and deionized (DI) water.

Table 1. Chemical compositions of the FeSi alloy (wt.%)

Alloy	Fe	Si	C	P	S	O	N
FeSi	Bal.	7.43	0.008	<0.003	<0.005	<0.001	<0.003

Three electrode electrochemical cell was performed[22]. The working electrode (WE) was an FeSi alloy plate (10 × 10 mm^2), The reference electrode (RE)was a Pt plate (Aladdin Chemical Reagent Co., Ltd.), and the counter electrode (CE) was a Li foil (Aladdin Chemical Reagent Co., Ltd.).

The electrolyte was prepared in an MBRAUN-UNIlab glove box. The glove box was filled with argon. DMC and EMC were weighed according to the volume ratio (DMC: EMC = 1:1), and then a mixed solution of DMC and EMC was added to the lithium salt. The lithium salt concentration was 1.0 M $LiPF_6$ and was battery grade (Zhuhai Guangrui New Material Co., Ltd.).

2.2 Electrochemical tests

Electrochemical performance was investigated by electrochemical workstation CS350 (Wuhan Corrtest Instruments Corp., Ltd.), which was mainly used to examine the polarization behavior of FeSi alloy. Cyclic voltammograms were noted at 0.1 $mV \cdot s^{-1}$ between 0 and 3 V. The potential scan was cycled three times in this potential range. Electrochemical impedance spectroscopy (EIS) was studied in the frequency range of 10^{-2} – 10^5 Hz with a signal amplitude of 10 mV. The polarization curves were evaluated from a potential range of 2 – 3 V at a sweeping rate of 1 $mV \cdot s^{-1}$. For weight loss measurements, the FeSi alloy plates (25 × 50 × 1 mm^3) were weighed using a HengJi analytical balance (PA1204) before and after corrosion, for which the readability is 0.1 mg. All measurements were tested at room temperature, 23 ± 2 ˚C (296 ± 2 K), under a dry Ar atmosphere. After tests, the morphology of the corrosion product layer was observed using the phenom G2 scanning electron microscope. Additionally, XPS was used to study species status.

3. RESULTS AND DISCUSSION

3.1 Corrosion behavior: gravimetric study

Figure 1 depicts the results of mass loss for three replicas at different immersion time. As Fig. 1 shows, the red line corresponds to the average mass loss of the FeSi alloy at different immersion time in 1.0 M $LiPF_6$ in EC/DEC solution, the red line shows that the increase in average mass loss reflects the dissolution of FeSi alloy in electrolyte; It can be seen from the blue line that the corrosion rate is a function of immersion time. These values in the scale on the right side of the figure are assumed rates of the dissolution of the FeSi alloy. The corrosion products must be removed by 40 kHz ultrasonic in acetone. Weight loss (Δm) was calculated by subtracting the initial weight from the final weight of the alloy. The average corrosion rate was calculated from the average of the three replicas. The corresponding standard deviations are reported. The corrosion rate (*V*) was calculated as follows (1):

$$V = \frac{\Delta W}{AT} \quad (1)$$

where V represents the corrosion rate ($mgcm^{-2}day^{-1}$), Δm as the difference between the mass loss before and after immersion (mg), *A represents* the sample contact area (cm^2) and T represents the immersion time (days).

Figure 1 shows that the corrosion rate is downward and the results indicate that the corrosion rate at 10 days reduced approximately 44.71% on the first day. The decay of corrosion rate may be due to the deposition of insoluble corrosion products on the electrode surface, which prevents the corrosive electrolyte from further corroding the FeSi alloy substrate. By comparing these two immersion stages, we can conclude that the corrosion process is fast and the thermodynamic versus kinetic reaction control of the cathodic reaction is in its early stages. The process of cathodic controlled corrosion is due to the strong oxidation ability of electrolyte, which leads to the dissolution of alloy. The partial dissolution of the oxidant in the FeSi alloy and the deposition of insoluble corrosion products on the electrode surface make the corrosion process transform anode control of the later immersion time.

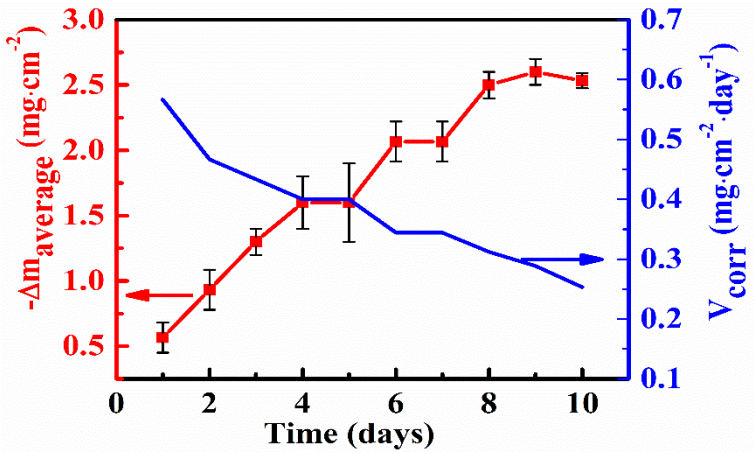

Figure 1. Corrosion rate and average mass loss curves of FeSi alloy in 1.0 M $LiPF_6$ solution at different immersion time (1 – 10 days).

3.2 Electrochemical test results

Cyclic voltammogram (CV) measurements of FeSi alloy processes were conducted in a voltage range of 0 – 3 V vs. Li/Li^+, and the scanning rate is 0.1 $mV \cdot s^{-1}$, as shown in Fig. 2. From the CV curve, the oxidation peaks of the alloy are 0.95 and 0.65 V vs. Li/Li^+, and the corresponding reduction peaks are 1.95 and 1.58 V vs. Li/Li^+ respectively. Particularly, the value of the current in a voltage range of 0.5 – 2.0 V vs. Li/Li^+ was reduced in the second and third cycles. Compared with the 2 nd and 3 rd CV curves, the 1 st CV Curve shows more obvious redox peaks and larger CV curve areas. The reduction of CV curve area shows that FeSi alloy electrode has irreversible capacity. The CV curve area of the 2 nd and 3 rd are close to each other, indicating that the FeSi alloy has relatively stable electrochemical properties in the electrolyte[23]. The cathode peak of 1 to2 V vs. Li/Li^+ is considered to be the interface between the reduction of FeSi alloy film to metal, the formation of Li_2O salt and the formation of the

solid electrolyte interfacial (SEI) layer[24]. Similar to the first CV curve, the obvious cathode peak at 1.58 V vs. Li/Li^+ in the second CV curve indicates that the film formed by the anode is reduced to metal. An obvious cathode peak at 0.65 V vs. Li/Li^+ is due to the under potential deposition (UPD) of lithium on the surface of FeSi alloy. In the anode direction, the anode peak at 0.95 V vs. Li/Li^+ is caused by the oxidation of deposited lithium. In the oxidation reaction direction, the anodic peak at 0.95 V vs. Li/Li^+ is caused by the oxidation of the deposited lithium. Both UPD and the corresponding oxidation of lithium were performed at lower potentials even though the redox potential was shifted slightly. Another obvious anodic peak appeared at 1.95 V vs. Li/Li^+, which is considered an oxidation process of FeSi alloy.

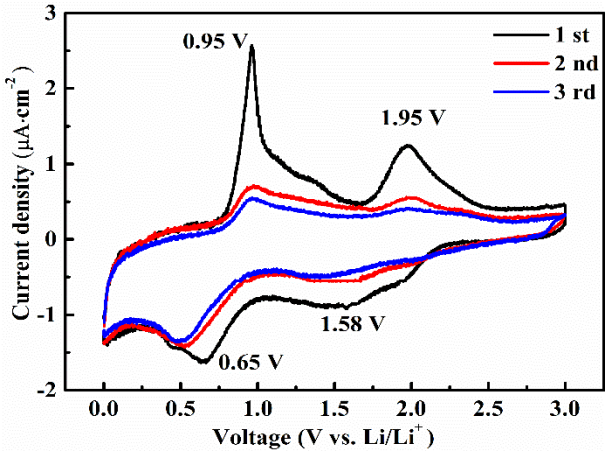

Figure 2. Cyclic voltammograms of FeSi alloy in 1.0 M $LiPF_6$ solution.

To further investigate the interfacial behavior of the FeSi alloy, electrochemical analysis was conducted to examine the Nyquist (Fig. 3a), phase-frequency (Fig. 3c) and bode (Fig. 3d) in the $LiPF_6$ solution after immersion time for 0 – 72 h. The impedance spectrum has a semicircular arc in the high frequency range. The high frequency capacitive arc resistance is controlled by the charge transfer process in the electric double layer formed between the metal surface and the corrosion medium. The semicircular arc is mainly formed on the surface of the electrode by a passive film, namely, the solid electrolyte interface (SEI). The diameter of the capacitive reactance arc is an important basis to investigate the corrosion resistance of materials. The larger the diameter of the capacitive reactance arc, the greater the electrochemical resistance. Fig. 3a shows that the Nyquist impedance spectrum depicts a semicircular arc within the frequency range examined. The radius of the semicircles also depends on the immersion time with the smallest radius for initial immersion. Generally, the value of EIS increases with the immersion time.

The inset in Fig. 3b shows the equivalent circuit and the EIS fitting parameters of the FeSi alloy are listed in Table 2. Rs represent serial resistance due to the solution and the electrode surface, CPE is typically considered the interface capacitance of electrode solution, Rct is the charge transfer resistance of the electric double layer and W (Warburg impedance) denotes an impedance caused by diffusion. Impedance spectra were fitted by an equivalent circuit diagram, and the accuracy of the fitting was evaluated via standard deviation chi-square. As Fig. 3a and Table 1 show, the FeSi alloy electrodes show

increaseing impedance values with an increase in immersion time. Furthermore, the phase-frequence plots showed in Fig. 3c obviously drawn there are two constants in the impedance spectrum at 72 h. It can be seen from the Fig. 3c that there is only one obvious characteristic peak at 0 − 48 h. In the initial state, the frequency of the characteristic peak is approximately 25 Hz. With an increase in immersion time, the characteristic peak moves to the left. At 72 h, there are two obvious characteristic peaks, with the frequencies of 1.74 Hz and 31.5 Hz respectively Therefore, it is considered that FeSi alloy has good corrosion resistance in the $LiPF_6$ solution.

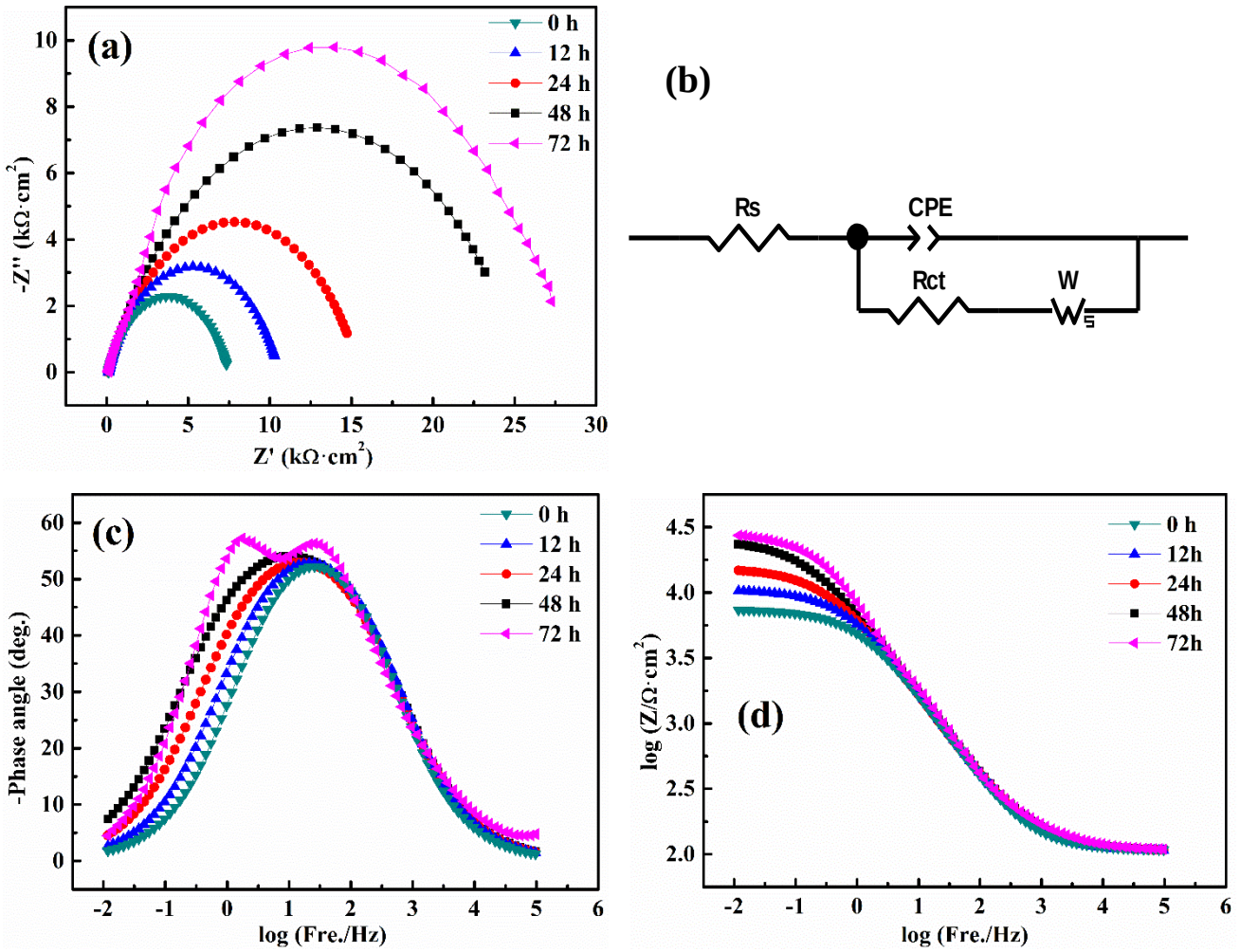

Figure 3. EIS diagrams of FeSi alloy in 1.0 M $LiPF_6$ solution at different immersion time (0 − 72 h). (a) Nyquist, (b) equivalent circuit, (c) phase-frequency, (d) bode plot.

Table 2. EIS fitting parameters of FeSi alloy in 1.0 M $LiPF_6$ solution at different immersion time (0 − 72 h).

Time (h)	Rs ($\Omega \cdot cm^2$)	CPE ($\Omega \cdot cm^2$)	Rct ($k\Omega \cdot cm^2$)	W ($k\Omega \cdot cm^2$)	Chi-square
0	103.60	3.32×10^{-5}	6.84	3.82	4.72×10^{-3}
12	104.70	3.47×10^{-5}	8.31	4.24	4.57×10^{-3}
24	105.70	3.78×10^{-5}	11.72	5.99	3.15×10^{-3}
48	106.80	3.66×10^{-5}	24.87	8.04	5.23×10^{-3}
72	109.20	3.67×10^{-5}	44.59	11.59	7.39×10^{-3}

Figure 4 shows the potentiodynamic polarization curves. According to the Tafel extrapolation method, the polarization curves were used to calculate the corrosion potential (Ecorr) and corrosion current (icorr) listed in Table 3. It showed that the corrosion current density and corrosion potential were various with different immersion time in 1.0 M $LiPF_6$ in EC/DEC mixture (1:1 ratio by volume) solution.

Obviously, it can be perceived that Ecorr increase from 2.11 to 2.58 V vs. Li/Li^+ with an increase in the immersion time, and it is suggested that FeSi alloy immersed for 0 h is more prone to corrosion than FeSi alloy immersed for 72 h.

Usually, icorr denotes the corrosion rate of of materials[25], and the value of every specimen can be calculated via Tafel extrapolation [26]. Table 3 shows the icorr value shifts from 0.63 to 0.08 $\mu A \cdot cm^{-2}$ with the increase of the immersion time. The phenomenon signifies an excellent corrosion resistance of FeSi alloy, which indicates the reduced corrosion tendency of FeSi alloy in 1.0 M $LiPF_6$ in EC/DEC mixture (1:1 ratio by volume) solution. The corrosion process gradually slows down. This result corresponds to gravimetric studies.

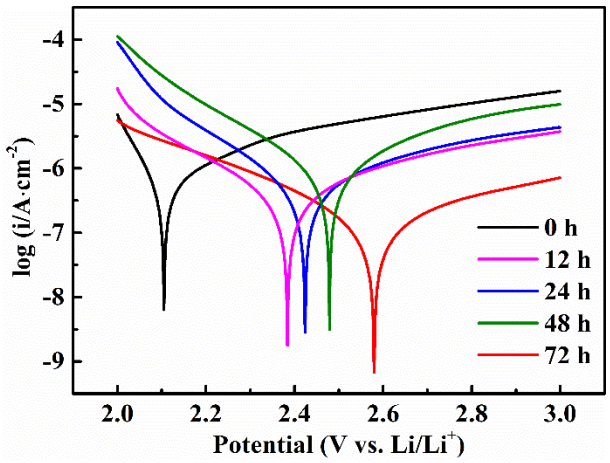

Figure 4. Polarization curves of FeSi alloy in 1.0 M $LiPF_6$ solution.at different immersion time (0 − 72 h).

Table 3. Ecorr and icorr values of FeSi alloy in 1.0 M $LiPF_6$ solution at different immersion time (0 − 72 h)

Time (h)	E_{corr} (V vs. Li/Li^+)	i_{corr} ($\mu A \cdot cm^{-2}$)
0	2.11	0.63
12	2.38	0.45
24	2.42	0.34
48	2.48	0.21
72	2.58	0.08

3.3 SEM analysis

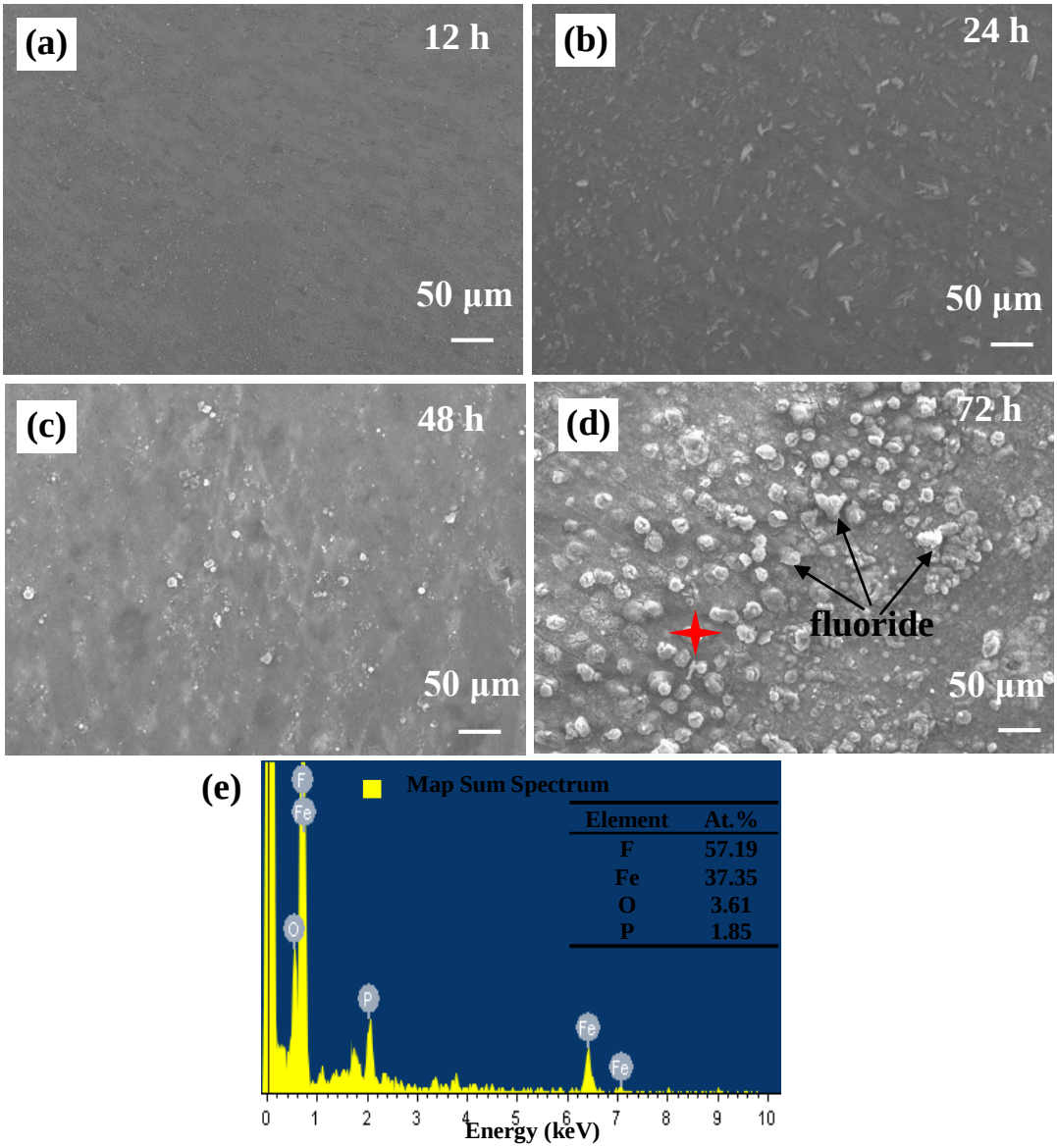

Figure 5. SEM images of FeSi alloys in 1.0 M $LiPF_6$ solution. (a − d) immersion time from 12 − 72 h. (e) EDS of the corrosion product.

For the barrier property of the corrosion product layer, it is important to investigate the morphology of the corrosion product layer formed on the surface of FeSi alloy with different immersion time in 1.0 M $LiPF_6$ solution. The morphology of the corrosion products of FeSi alloys in 1.0 M LiPF6 solution shown in Fig. 5. The smooth and uniform coating (Fig. 5a) evolves into a heterogeneous structure after 12 h of immersion, as shown in Fig. 5b. After 48 h of immersion, it is covered by corrosion products in some areas and corrosion product particles gradually become larger (Fig. 5d). It is worth notice that there are a large number of white particles are distributed on the FeSi alloy surface (Fig. 5d) and obvious particle aggregation occurred. And the corrosion products were evenly covered at last. The EDS result Fig. 5e shows the corrosion product layer is mainly composed of fluoride, which will be precipitated because of lower solubility of the metal fluorides[27]. The presence of extra the corrosion products layer can reduce the contact area between the material and electrolyte, and could prevent further corrosion of FeSi alloy surface by corrosive electrolyte[28, 29]. Thus, the occurrence of corrosion process is slowed down or inhibited, and the electrochemical performance of the material is more stable, which is in agreement with Fig. 1 and Fig. 4 that the FeSi alloy shifts from the cathode to anode.

3.4 XPS analysis

The above gravimetric and electrochemical test results indicate that the $LiPF_6$ solution corrodes the iron matrix of the FeSi alloy electrode. The corrosion mechanism and the accumulated corrosion products of FeSi alloy was further studied by XPS. Fig. 6 shows XPS spectra of corroded FeSi alloy with 72 h immersion time in 1.0 M $LiPF_6$ in EC/DEC mixture (1:1 ratio by volume) solution.

In order to obtain more detailed information, first, the chemical composition of the sample was thoroughly analyzed via XPS, and a series of spectra were obtained to determine the content of surface elements such as Si, P, F, O and C in the sample (Fig. 6). XPS measurements of FeSi alloy processes were conducted in a binding energy range of 0 − 1400 eV. The main elements on the surfaces of Fe, P, F, O and C after corrosion of Fe Si alloy were scanned and measured, and calibrated with standard C1 peak at binding energy was 284.8. However, no XPS peak of Si element was observed. It means that each layer is dominated by iron concentration, indicating that the surface layer (corrosion product) is mainly composed of iron-based materials. The composition and oxidation state of Fe and F elements were investigated by deep level XPS. The results presented above (Fig6. b and c) clearly show that the electrolyte corrodes the FeSi alloy substrate. The results show that the high oxidation state of the P^{5+} atom in $LiPF_6$ makes $LiPF_6$ an oxidant, resulting in the corrosion of the FeSi alloy, and LiF a byproduct of the corrosion process via Eq. (2)[19].

$$xM+PF_6^- \rightarrow M_xF_2+PF_3+F^- \quad (2)$$

Therefore, XPS data are helpful in clarifying the corrosion mechanism of these products. The binding energy related to F1s can explain the chemical state of atoms in the corrosion product layer. Fig. 6b presents the corresponding deconvolution peaks. Note that the peak obtained after 72 h of corrosion has two deconvolution peaks. The peak at 687.4 eV indicates the existence of redundant $LiPF_6$. Additionally, the main peak at 685.3 eV indicates the existence of FeF_2 and LiF, and the presence of FeF_2 and LiF also via Eq. (2).

Additionally, because XPS can help distinguish oxidation states, Fe2p XPS spectra were also investigated (Fig. 6c). From the deconvolution peak of the spectrum, iron has three oxidation states (Fe^0, Fe^{2+} and Fe^{3+}). Fe^{2+} indicates the partial dissolution of ferrosilicon alloy, as determined via Eq. (2). Fe^{3+} mainly corresponds to the further re-oxidation of Fe^{2+} formed by the dissolution of FeSi alloy, as schematized in Eq. (3).

$$2FeF_2+PF_6^- \rightarrow 2FeF_3+PF_3+F^- \quad (3)$$

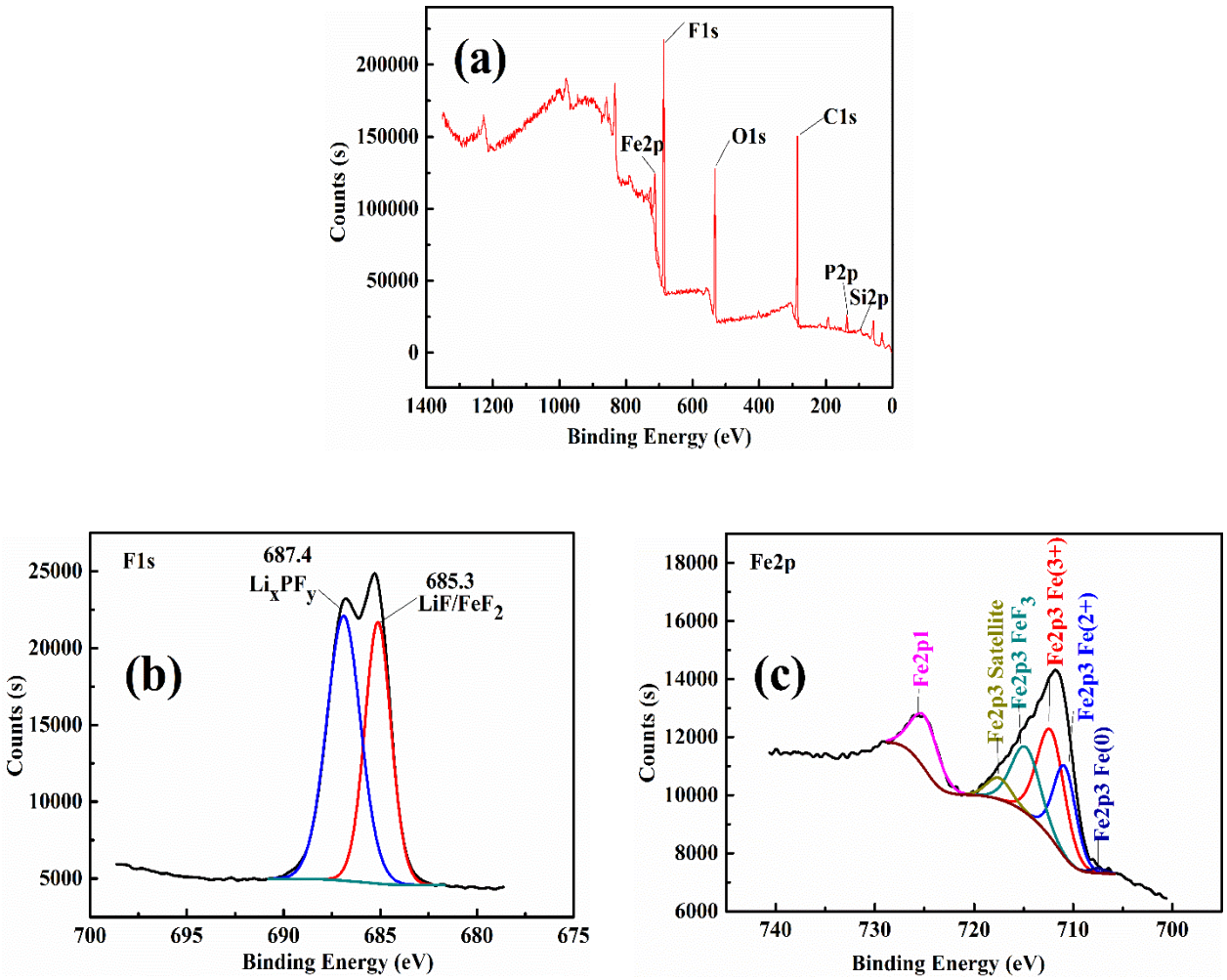

Figure 6. XPS spectra of corroded FeSi alloy in 1.0 M $LiPF_6$ solution at 72 h immersion time. (a) Survey spectrum, (b) F1s spectra at 72 h, (c) Fe2p spectra at 72 h.

3.5 XRD analysis

The corresponding XRD patterns were used to study the phase of the corrosion product layer of FeSi alloy, as shown in Fig. 7. All samples exhibit α-$FeSi_2$ and β-$FeSi_2$ phases based on the figure[30-32]. Moreover, two components were detected containing FeF_3 phase and LiF phase in the corroded specimen[33].

Hence, the surface corrosion products should be mainly LiF and FeF_3. Conversely, the relative intensities of the characteristic peaks of surface corrosion products in Fig. 7 show an increasing trend as the immersion time increases.

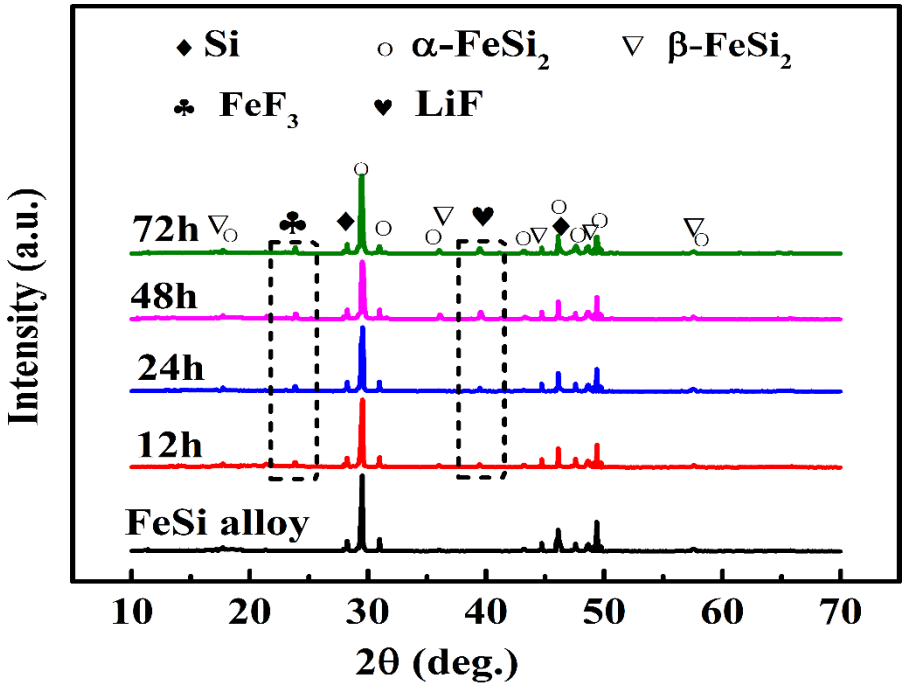

Figure 7. XRD patterns of corroded FeSi alloy in 1.0 M $LiPF_6$ solution at different immersion time.

As stated above, the results for the X-ray diffraction patterns of the corrosion product layers presented in this research confirm the presence of fluoride layers.

The $LiPF_6$-based electrolyte always contains a little bit of water, which consequently breakdown the electrolyte. Then, the byproducts would be generated FeF_3 and LiF via Eq. (2). In $LiPF_6$ solution, the outer surface of FeSi alloy was formed with iron (III) fluoride layer, which will be precipitated because of lower solubility of the metal fluorides[34]. Thus, the occurrence of corrosion process is inhibited. Thereby, the corrosion product layer deposited on the surface of FeSi alloy played an important role in corrosion resistance.

4. CONCLUSIONS

The corrosion and interfacial behavior of FeSi alloy electrodes was examined in 1.0 M $LiPF_6$ in EC/DEC mixture (1:1 ratio by volume) solution. The obtained results are summarized as follows.

(1) The electrochemical and gravimetric data show that the corrosion rate at 10 days decreases to approximately 44.71% of the initial value; thus, the corrosion rate decreases as the immersion time increases, and FeSi alloy has good electrochemical stability in the electrolyte.

(2) The corrosion behavior of FeSi alloy is mainly caused by the dissolution of iron. PF_6^- in $LiPF_6$ solution as an F^- source corroded Fe (0) to Fe (II) that further evolve into Fe (III), forming fluoride

films (FeF_3) at the alloy surface. FeF_3 can enhance the protection performance of the corrosion product film against the corrosion of FeSi substrate.

(3) A passivating film of iron (III) fluoride film accumulates on the electrode surface, preventing further corrosion of the electrode by the electrolyte and hindering corrosion, thereby improving the corrosion resistance of the material.

ACKNOWLEDGMENTS
This work was supported by the special funds for the construction of an innovative province of Hunan (2019GK2231).

References

1. M. Armand, J.M. Tarascon, *Nature*, 451 (2008) 652.
2. G.E. Blomgren, *J. Electrochem. Soc.*, 164 (2017) A5019.
3. Ren, J. Guo, C. Wang, Q.H. Wu, X. Liu, Y. Yang, L. He, W. Zhang. *Nanoscale*, 6 (2014) 3353.
4. Y. Chen, Y. Yuan, C. Xu, L. Bao, T. Yang, D. Ning, Y.F. Lin, H.W. Zhang, *J. Mater. Sci.*, 55 (2020) 13938.
5. B. Wang, J. Ryu, J.A. Choi, X. Zhang, D. Pribat, X. Li, L. Zhi , S. Park, R.S. Ruoff, *ACS Nano*, 13 (2019) 2307.
6. M. Salah, C. Hall, P. Murphy, C. Francis, R. Kerr, B. Stoehr, S. Rudd, M. Fabretto, *J. Power Sources*, 506 (2021) 230194.
7. J. Zeng, N. Fu, X. Wang, A. Zhou, Z. Yang, *Appl. Surf. Sci.*, 557 (2021) 149860.
8. M. Jiao, Y. Wang, C. Ye, C. Wang, W. Zhang, C. Liang, *J. Alloys Compd.* 842 (2020) 155774.
9. Z. Lu, B. Li, D. Yang, H. Lv, M. Xue, C. Zhang, *Rsc Adv.*, 8 (2018) 3477.
10. G. Zhu, W. Luo, L. Wang, W. Jiang, J. Yang, *J. Mater. Chem.*, 7 (2019) 24715.
11. J. Xie, L. Tong, L. Su, Y. Xu, L. Wang, Y. Wang, *J. Power Sources,* 342 (2017) 529.
12. M. Zhang, L. Li, L. Jian, S. Zhang, Y.Y. Shang, T.T. Xu, S.G. Dai, J.M. Xu, D.Z. Kong, Y. Wang, X.C. Wang, *J. Alloys Compd.,* 878 (2021) 160396.
13. I. Kang, J. Jang, K.W. Yi, Y.W. Cho, *J. Alloys Compd.*, 770 (2019) 369..
14. J. Xie, H. Zhang, J.Chu, W.Shen, R.Chen,J.Yu, *J. Alloys Compd.*,768 (2018) 1072.
15. H.Y. Lee, S.M. Lee, *J. Power Sources*, 112 (2002) 649.
16. E. Zinigrad, L. Larush-Asraf, J.S. Gnanaraj, M. Sprecher, D. Aurbach, *Thermochim. Acta,* 438 (2005) 184.
17. N. Schulz, R. Hausbrand, C. Wittich, L. Dimesso, W. Jaegermann, *J. Electrochem. Soc.*, 165 (2018) A833.
18. Z. Xiao, C. Yu, X. Lin, X. Chen, C. Zhang, H. Jiang, F. Wei, *Catal. Today*, 364 (2021) 61.
19. B. Guitian, X.R. Novoa, A. Pintos, *Electrochim. Acta,* 304 (2019) 428.
20. C.L. Li, S.W. Zeng, P. Wang, Z.J. Li, Y. Li, D.N. Zhao, J. Wang, H.N. Liu, S.Y. Li, *Trans. Nonferrous Met. Soc. China,* 31 (2021) 1439.
21. J. Chen, Y. Zhao, H Gao, S. Chen, W. Li, X. Liu, X. Hu, S. Yan, *Surf. Coat. Tech.,* 421 (2021) 127369.
22. X. He, S. Schmohl, H.D. Wiemhöfer, *Polym. Test.,* 76 (2019) 505.
23. S.T. Myunga, Y. Sasakia, T. Saitob, Y.K. Sunc, H. Yashiro, *Electrochim. Acta,* 54 (2009) 5804.
24. B. Liang, S. Zhu, J. Wang, X. Liang, H. Huang, D. Huang, W. Zhou, S. Xu, J. Guo, *Appl. Surf. Sci.*, 550 (2021) 149330.
25. Y. Guo, R. Ali, X. Zhang, W. Tian, L. Zhang, H. Lu, X. Jian, J. Xie, L. Deng, *J. Alloys Compd.,*

834 (2020) 155075.
26. Z. Shi, M. Liu, A. Atrens, *Corros. Sci.,* 52 (2010) 579.
27. Y. Kerroum, S. Skal, A. Guenbour, A. Bellaouchou, R. Boulif, J.G. Anton, A. Zarrouk, *Surf. Interfaces* ,19 (2020) 100481.
28. M. Xu, H.D. Dewald, *Microchem. J.,* 81 (2005) 225.
29. J.A. Choi, D.W. Kim, Y.S. Bae, S.W. Song, S.H. Hong, S.M. Lee, *Electrochim. Acta*, 56 (2011) 9818.
30. H.Y. Lee, S.M. Lee, *J. Power Sources,* 112 (2002) 649.
31. K. Adpakpang, J.E. Park, S.M. Oh, S.J. Kim, S.J. Hwang, *Electrochim. Acta*, 136 (2014) 483.
32. T. Li, Y.L.Cao, X.P. Ai, H.X. Yang, *J. Power Sources*, 184 (2008) 473.
33. X. Zhou, H. Sun, H. Zhou, *J. Electroanal.Chem.,* 810 (2018) 41.
34. K. Furukawa, N. Yoshimoto, M. Egashira, M. Morita, *Electrochim. Acta,* 140 (2014) 125